DOI:
10.1116/6.0000561

Document Version
Peer reviewed version

Cholesterol Content in the Membrane Promotes Key Lipid-Protein Interactions in a Pentameric Serotonin-Gated Ion Channel

Alessandro Crnjar[1, a)] and Carla Molteni[1, b)]
Physics Department, King's College London, Strand, London WC2R 2LS, United Kingdom.

(Dated: 10 October 2020)

Pentameric ligand-gated ion channels (pLGICs), embedded in the lipid membranes of nerve cells, mediate fast synaptic transmission and are major pharmaceutical targets. Because of their complexity and the limited knowledge of their structure, their working mechanisms have still to be fully unravelled at the molecular level. Over the past years, evidence that the lipid membrane may modulate the function of membrane proteins, including pLGICs, has emerged. Here we investigate, by means of molecular dynamics simulations, the behaviour of the lipid membrane at the interface with the 5-HT_{3A} receptor (5-HT_{3A}R), a representative pLGIC which is the target of nausea-suppressant drugs, in a non-conductive state. Three lipid compositions are studied, spanning different concentrations of the phospholipids POPC and POPE and of cholesterol, hence a range of viscosities. A variety of lipid interactions and persistent binding events to different parts of the receptor are revealed in the investigated models, providing snapshots of the dynamical environment at the membrane-receptor interface. Some of these events result in lipid intercalation within the transmembrane domain and others reach out to protein key sections for signal transmission and receptor activation, such as the Cys-loop and the M2-M3 loop. In particular, phospholipids, with their long hydrophobic tails, play an important role role in these interactions, potentially providing a bridge between these two structures. A higher cholesterol content appears to promote lipid persistent binding to the receptor.

I. INTRODUCTION

Pentameric ligand-gated ion channels (pLGICs) are involved in fast synaptic transmission and, as such, are crucial drug targets, often investigated for the development of novel pharmaceuticals. These neuroreceptors are embedded in the lipid membrane of nerve cells, and they have characteristic structural features: they are made up of five subunits around an ion-permeable channel, divided into an extracellular domain (ECD), a transmembrane domain (TMD) and often an intracellular domain (ICD). The binding of neurotransmitters at the interface between subunits in the ECD is associated with the opening of the channel within the TMD, thus allowing the flux of ions between the extracellular environment and the cytosol of the cell.[1,2] Many open questions still remain about the mechanistic functioning of these proteins, in particular related to the transmission of the mechanical signal, initiated by neurotransmitter binding, which triggers the opening (gating) of the channel. Despite the recent increasing number of good resolution X-ray and cryo-electron microscopy structures (either of full or partial length, apo or bound, and in different functional states),[3–16] addressing these issues is far from trivial due to protein complexity.

While the ligand orthosteric binding to the ECD remains the ultimate trigger for channel gating, there is growing evidence that the lipid membrane may contribute to the overall mechanisms through the interactions at the membrane-receptor interface. Lipids interactions have been suggested to affect structural and dynamical features in several membrane proteins. These include pLGICs,[17,18] such as the nicotinic acetylcholine receptor (nAChR) which has been the most studied in this context,[19–25]the 5-hydroxytryptamine type 3A receptor (5-HT_{3A}R),[26] the $GABA_A$ receptor,[27] the Glycine receptor,[28] the prokaryotic *Erwinia chrysantemi* (ELIC) ion channel[29–31] and *Gloeobacter violaceous* (GLIC) receptor,[32,33] as well as G-protein coupled receptors (GPCRs),[34–37] mechanosensitive channels,[38], amyloid precursor proteins,[39] heterotrimeric G proteins,[39,40] and others. However, the mechanisms underlying these lipid-modulated effects in pLGICs are still poorly understood;[18] hence, additional investigations, including atomistic simulations, are needed to build a reliable picture at the molecular level, especially in cases where very few studies have been performed so far, such as for the 5-HT_{3A} receptor.[26]

The cell membrane is very complex to model, with the "average" human membrane estimated to contain over 60 lipid species.[41] Although great progress has been made in realistically modelling the cell membrane at various levels of resolution (from atomistic to coarse grained and super coarse grained),[42] even simplified models, going beyond a single lipid species, pose challenges to state-of-the-art simulations, but can provide interesting preliminary insights into the receptor-membrane interface.

Phospholipids, as well as cholesterol (CHL), are major components of animal cell membranes. In particular, 1-palmitoyl-2-oleoyl-sn-glycero-3-phosphocholine (POPC) and 1-Palmitoyl-2-oleoyl-sn-glycero-3-phosphoethanolamine (POPE) are prevalent phosphatidylcholines and phosphatidylethanolamines respectively. POPC, POPE and CHL are represented in Fig. 1. POPC is a neutral phospholipid made up of two hydrophobic tails joined to a hydrophilic head group which incorporates a choline, and only differs from POPE in the head group, which for the latter consists of an ethanolamine. Thus, POPC and POPE have different abilities to form hydrogen bonds. This has been demonstrated to affect, among others, the structural conformation of the mycobacterium tuberculosis mechanosensitive

a)Electronic mail: alessandro.crnjar@kcl.ac.uk
b)Electronic mail: carla.molteni@kcl.ac.uk

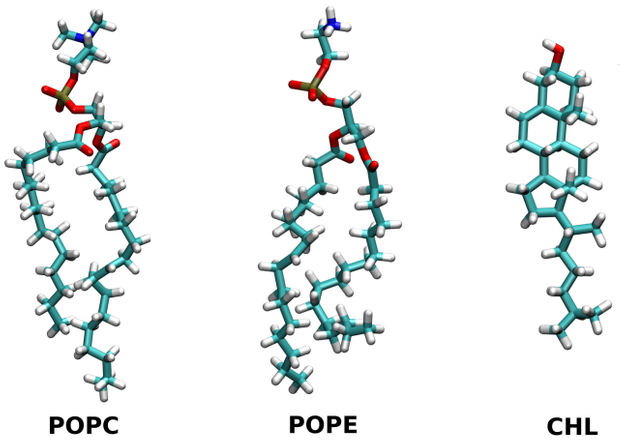

FIG. 1. Structure of POPC (left), POPE (centre), and cholesterol (CHL, right).

channel, in molecular dynamics (MD) simulations of such protein embedded in POPE membranes, manually turned into POPC during the simulation.[38] Pure-POPC membrane have also been proved, by means of single-particle cryo-electron microscopy, to decouple the ECD and the TMD of ELIC, thus preventing the mechanical signal induced by agonist binding to propagate into the latter; POPC polar heads were found responsible, as supported by MD simulations, of lipid-protein interactions which affect the closed-open-desensitized equilibrium constants.[29] Native mass spectrometry, coarse-grained simulations and functional assays found the glycerophospholipid POPG binding to ELIC responsible for the stabilization of its open state with respect to the desensitized state.[30] Receptor reconstruction in high-density-lipoparticles of a GPCR proved how the head group of phospholipids can affect agonist and antagonist binding and receptor activation.[37] A comparison of the X-ray structures of the *Caenorhabditis elegans* glutamate-gated chloride channel (GluCl) in apo-state and in a POPC-bound state revealed how lipids can potentiate agonist binding and promote an expanded open-like conformation of the transmembrane domain.[7] The combination of POPC and POPE phospholipids (with the addition of CHL) has been extensively used *in-silico* works[26,33–35,38,43,44]. It is a good exploratory minimal but representative choice, and is used here, although it is not unique. In fact, other choices are possible, for example by considering phospholipids with the same head group but different hydrophobic tails, like POPC and SDPC[26], or more complex compositions within a coarse-grained treatment.[28]

Cholesterol has a much shorter structure than POPC and POPE, being made up of four aromatic rings, an aliphatic tail and a hydroxyl group head. It is very important because it is found in high concentrations in the membranes of human brain cells.[45,46] When present in lipid membranes, cholesterol modulates membrane fluidity, affecting the lateral diffusion of phospholipids.[47] It typically binds to membrane proteins in preferred sites, referred to as "Cholesterol Recognition/interaction Amino acid Consensus sequence", or "CRAC" domains, and as "inverted CRAC" ("CARC") domains.[19,48–50] The sequence of CRAC domains is (L/V)-X_{1-5}-(Y)-X_{1-5}-(K/R) in the N-terminus to C-terminus direction, where L/V is either a leucine or a valine, X_{1-5} is any number between 1 and 5 of any amino-acid, Y is a tyrosine, and K/R is either a lysine or an arginine. The sequence of the CARC domain is instead (K/R)-X_{1-5}-(Y/F)-X_{1-5}-(L/V), from the N-terminus to the C-terminus. Cholesterol is able to affect various features of membrane proteins. For example, in the G-protein coupled 5-HT_{1B} receptor, its interaction with a transmembrane helix was found to modify the serotonin binding mode in the extracellular pocket by MD simulations.[44] In the 5-HT_{3A} receptor, microseconds-long simulations showed that cholesterol, with phospholipids POPC and SDPC, was able to penetrate into one subunit of the TMD during rearrangements upon serotonin-binding, contributing to the stabilization of an alleged pre-active state (i.e. a conformation which resembles an initial stage of channel opening), supporting its necessity in contrast to pure-POPC membranes.[26] In the adenosine type 2A receptor, cholesterol binding was found to affect, in *in-silico* studies, the binding poses of caffeine and its mobility in the pocket.[43]. Other *in-silico* investigations suggested that cholesterol binding may promote pore opening in the $GABA_A$ receptor[27] and is necessary for the structure preservation of the nicotinic acetylcholine receptor by promoting contacts between the ligand-binding domain and the pore.[21]

A conspicuous literature on pLGICs also suggests that the outermost M4 helix may act as a lipid sensor. This is the case of the nicotinic acetylcoline receptor, whose M4/Cys-loop interactions were suggested to be favoured by lipid-dependent properties through experimental characterisation.[24] Also in nAChR, the thickness of phosphatidylcholine membranes was experimentally shown to affect transitions between uncoupled and coupled conformations.[25] In ELIC, the M4 helix carries a lipid-binding site, whose disruption accelerates desensitization, as pointed out by mutagenesis experiments.[31]

Overall, the consensus is that various types of lipids, in particular phospholipids and cholesterol, are able to affect the function of a variety of membrane proteins, including pLGICs, because of their ability to bind to them, and thus act as potential mediators between different protein domains and/or alter the properties of such domains.

Here, we investigated, for different lipid compositions, the interface between model membranes and the 5-HT_{3A} receptor (5-HT_{3A}R), an important pLGIC which is involved in neurological diseases such as schizofrenia, Alzheimer's and many others, and is the target of nausea-suppressant drugs. This receptor belongs to the Cys-loop superfamily of pLGICs, which takes its name from the highly conserved Cys-loop at the interface between ECD and TMD. We carried out this study via all-atom MD simulations, with a pure-POPC membrane and two POPC-POPE-CHL mixed membranes of increasing viscosity. We characterized the interface between the receptor and the lipid membrane, through analysis of the occurrence of their interactions and the lipids proximity lifetime distributions. We observed several sustained binding events, some

of which involved lipid intercalation within the protein and/or interactions with relevant protein sections. We showed how cholesterol, which increases the viscosity of the lipid membrane, promotes lipid binding to the protein. We also showed how phospholipids may act as bridges between key protein sections, such as the Cys-loop and the M2-M3 loop, connecting the ECD and the TMD. Most previous MD studies of the 5-HT_3 receptor used single lipid membranes,[15,16,51–54] with the exception of a very recent study where a specific POPC/SPDC/CHL membrane composition was assessed against POPC and in the presence of neurotransmitters.[26]

II. METHODS

A homopentameric model of the mouse 5-HT_{3A} receptor was built from the X-ray apo-structure at 3.5 Å resolution determined by Hassaine et al. (PDB entry: 4PIR)[8] and is shown in Fig.2. The TMD is of particular relevance for the scope of this work, and is represented in Fig. 2 b) in a view orthogonal to the ion channel: it is made up of 4 helices per subunit, labelled M1, M2, M3, and M4 according to the progression alongside the primary sequence. The M1 and M3 helices are found at the interfaces between adjacent subunits. The M2 helices line the ion channel, and have therefore little chance to interact with the membrane, while the M4 helices occupy the outermost position facing the membrane.

The channel size at the hydrophobic gate, and the presence of Llama-derived single-chain antibodies (VHH) used to stabilize the structure during crystallization (which act as antagonists), suggest ions would not pass through and thus the structure is in a non-conductive state. Four residues in the M2-M3 loop (Thr276, Ala277, Ile278 and Gly279) were manually added as they were not resolved experimentally, and optimized with NQ-flipper, a web-based server for the analysis of rotamers.[55] Stabilizing agents and non-native fragments were not included. The ICD was only partially resolved, so, to avoid arbitrary reconstructions or imposing constraints, the terminal MA and MX helices were removed. The removal of the ICD allows for a considerable speed-up of the calculations, under the assumption that it does not exert a considerable influence on the lipid-protein interactions, which involve mostly the TMD, in the time scales explored here. The M3 and M4 helices were connected to each other through a short link of sequence VHKQDLQRD, which originally belonged to the link between M3 and MX. Its length was chosen so to match the M4 connection and to resemble the structure of ICD-lacking pLGICs, such as ELIC and GluCl.

The model was protonated at neutral pH, and embedded in lipid bilayers with the CHARMM-GUI membrane builder.[56] Three different membrane models were built, here labelled A, B and C: model A contains only POPC, model B contains 35% POPC, 35% POPE and 30% cholesterol, and model C contains 25% POPC, 25% POPE, and 50% cholesterol. The resulting membrane areas were about 125 Å by 128 Å for model A, 122 Å by 123 Å for model B, and 121 Å by 122 Å for model C. The pure-POPC model A is the least complex, resembles systems previously simulated,[51,53,54] and is thus a reliable standard for the comparison with the two mixed models. Model B has a 6:7:7 concentration, which has been used in past simulations of membranes with cholesterol (6), POPC (7) and a third lipid (7) for the study of serotonin receptors.[26,57] Model B represents an intermediate composition where cholesterol is present, but the phospholipids are still predominant. Model C has the highest percentage of cholesterol, which represents the upper CHL concentration in synaptic membranes (whose cholesterol content varies between 33% and 50%),[43,45,46] and would also prove useful for enhancing the sampling of cholesterol-related phenomena. The viscosity of the lipid bilayers increases from A to C.

The systems were then solvated in orthorhombic supercells, with a 15 Å buffer of TIP3P water and 0.15 M of Na^+ and Cl^- ions to reproduce physiological conditions. The final 5-HT_{3A}R models contained 183,207 atoms (model A), 182,877 atoms (model B), and 175,904 atoms (model C), including the ions and the solvent. The preparation procedure described so far is similar to that we previously used for a model 5-HT_{3A}R in a POPC bilayer where we studied a *trans-cis* proline molecular switch at room temperature.[54]

The systems were simulated with the NAMD 2.9 MD package[58] and the AMBER ff14SB[59] and LIPID14 forcefield.[60] The simulation time step was 2 fs, and the bonds containing hydrogen were constrained with the SHAKE algorithm. Particle Mesh Ewald was used for the electrostatic interactions and a cut off of 10 Å was employed for the non-bonded interactions.

The three models initially underwent a minimisation procedure, a slow heating up to 310 K and a partially restrained equilibration (with the protein α carbons restrained and the lipids free to diffuse). This equilibration phase lasted for 100 ns, as prescribed for the equilibration of lipid membranes whose typical diffusion occur over times of the order of tens to hundreds of nanoseconds,[61,62] and was necessary to preserve the non-conductive state and avoid unphysical conformational changes in the mixed membrane systems. The restraints were subsequently released. A subsequent unrestrained simulation was carried out within the isothermal-isobaric (NPT) ensemble for each model at a temperature of 310 K, which is above the gel transition temperature for all lipid species considered,[63,64] and at a pressure of 1 atm. The temperature was controlled by means of a Langevin thermostat with a collision frequency of 1.0 ps, and the pressure was controlled by means of a Langevin piston barostat with an oscillation period of 200 fs and a damping time constant of 100 fs.

For each of the three models, two replicas were carried out, with no restraints, for the production starting from the same initial geometries but with different initial velocities: one of 500 ns (RX), and one of 250 ns (RY). As lipids diffuse differently in separate replicas, this allowed us to explore additional statistics of the processes of lipid diffusion and lipid-protein interaction. For both RX and RY, the first 50 ns were excluded from statistics collection so to mitigate the use of the same initial geometry and allow for independent equilibration: thus the production runs lasted 450 ns for RX and 200 ns for RY.

There are different ways to improve statistics when performing simulations, for example long runs or multiple repli-

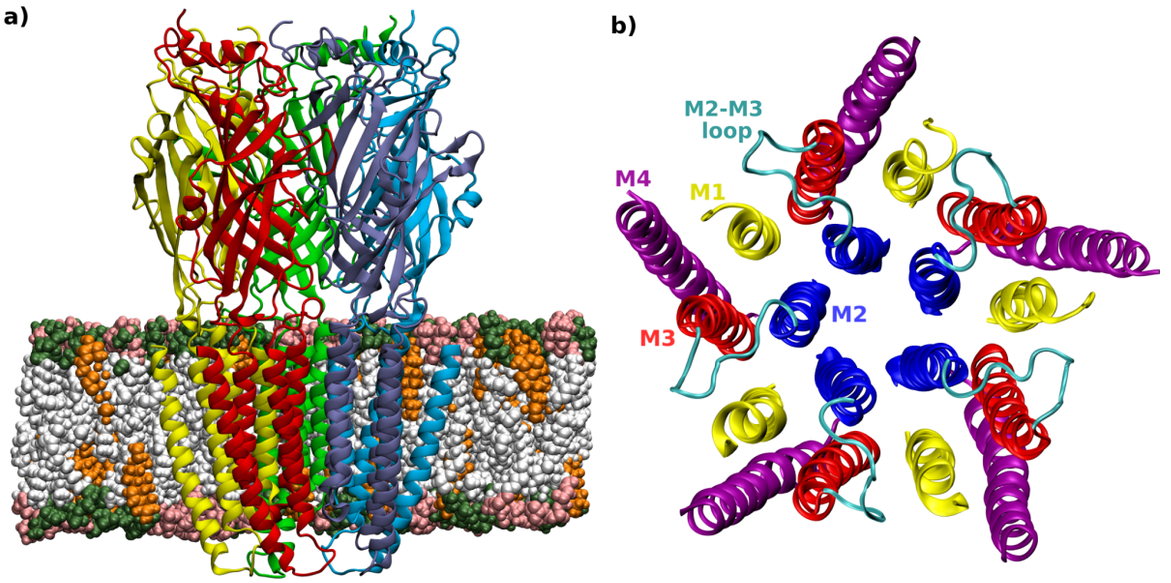

FIG. 2. a) The model of 5-HT$_{3A}$R embedded in the mixed membrane of model B (35% POPC, 35% POPE and 30% CHL). Pink: POPC heads; dark green: POPE heads; grey: POPC and POPE tails; orange: cholesterol. The five subunits are numbered in anticlockwise order as 1 in red, 2 in yellow, 3 in green, 4 in light blue and 5 in blue. b) View, orthogonal to the ion channel, of the transmembrane domain helices: M1 (yellow), M2 (blue), M3 (red) and M4 (purple). The M2-M3 loop is shown in green. The other loops connecting helices are not shown for simplicity.

cas of shorter simulations. To test whether these two approaches, in the case of similar computational cost, give qualitative similar results for time- and subunit-averaged quantities for the systems studied here, we performed some analysis over the average of the 50-to-250 ns time-windows of RX and RY (RXY400), and over the time window 50-to-450 ns of replica RX (RX400). Other analysis (specifically those that explicitly express an observable as a function of time) were performed over the 50-to-500 ns window of RX (RX450) and over the 50-to-250 ns window of RY (RY200).

Trajectories were sampled every 50 ps and analyzed with the Cpptraj[65] and MDAnalysis[66,67] software. Hydrogen bonds were identified by a donor-acceptor distance smaller than 3.5 Å and by a donor-hydrogen-acceptor angle larger than 120°. These values have been used in a variety of previous works in pLGICs[54,68–73] and are the defaults of analysis software such as MDAnalysis.[66,67]

III. RESULTS

The stability of the protein was assessed by means of the root mean square displacement (RMSD) of the backbone atoms with respect to the first frame of the unrestrained NPT simulations. Its evolution over time during the unrestrained dynamics is reported in the Supplementary information (SI) for the whole receptor, ECD and TMD (SI Figs. 1-3). The average RMSD over the production run, separately calculated for RXY400 and RX400, is shown in SI Fig. 4 for different parts of the protein: the ECD, the TMD, and the protein as a whole, and for each of the four TMD helices. The sequence of the substructures was defined as in Ref.[8]. The three models result stable, and both averaging methods provide similar results. A degree of variability was observed among the five subunits, which reflects statistical sampling and fluctuations within the isothermal-isobaric ensemble, and different local lipid environments around the TMD. The models maintained structural integrity during the simulations.

Since the M4s are the outermost helices, they move more than the other three types of TMD helices, as expected, with the largest fluctuations determined by their terminals which extend outside the membrane. Our 5-HT$_{3A}$ model does not include the intracellular domain, which being incomplete, would have produced fairly large fluctuations if left unrestrained.

The lipid bilayers of three models exhibit the expected relative viscosities, as qualitatively shown by the lipid lateral mean square displacements (MSD) in SI Fig. 5: model C is the most viscous, having the highest content of cholesterol, while model A is the least viscous. Lateral diffusion coefficients were evaluated via Einstein's equation providing values of the order of $\mu m^2 s^{-1}$, in agreement with previous calculations of lipid systems.[20,74,75] The absolute values are affected by the use of Langevin dynamics, time-scale, size of the membrane and presence of the embedded protein.

In order to characterise in details the protein-membrane interface, we calculated the distributions of proximity lifetimes of those lipids with any atom within 3.5 Å of the re-

ceptor transmembrane domain (Fig. 3), as the lipids characterised by high proximity lifetimes form the most stable interactions with the protein. Since the lifetimes depend on the specific replica, these distributions were separately calculated for RX450 and RY200. We considered multiple time windows shifted by 5 ns, and calculated averages and standard deviations for each 5 ns time period. The statistics available for each residence time decreases for larger times.

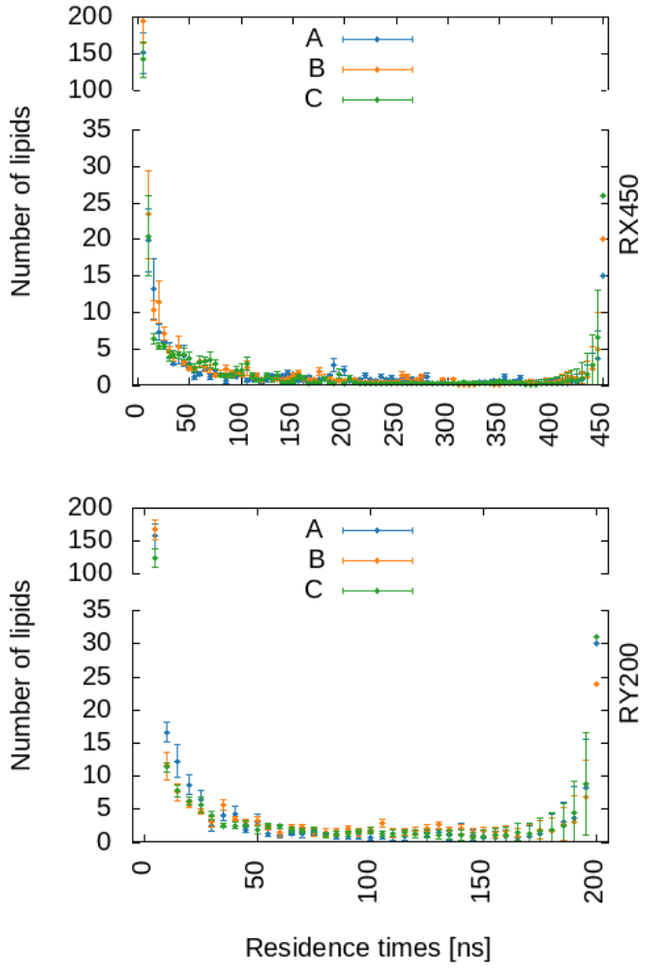

FIG. 3. Proximity lifetimes of any lipid in close proximity to the TMD in model A (blue), model B (orange) and model C (green) for RX450 (top) and RY200 (bottom).

The distributions for the three models decay fast well before 50 ns, implying that very few lipids spend relatively long times close to the protein. However, the value of the histogram corresponding to the longest time sampled is higher, which means that a certain amount of lipids spent the entire production time attached to the receptor. These lipids were further investigated: SI Figs. 6 to 11 show their root mean square fluctuations (RMSF) for the three models, calculated over RX450 and RY200 with respect to their average positions. The RMSFs of phospholipids were calculated separately for the head and the two tails, as each of these parts may display different mobility due to specific interactions with or hindrance by the protein and/or other lipids. The investigated lipids are characterised by different RMSF values, ranging from about 1.5 to about 8.5 Å. Their number varies both among models and between replicas. The number of lipid residues that stay attached for the whole production to the protein, and at the same time are characterized by low fluctuations (i.e. smaller than 3.0 Å), are shown in Table I.

TABLE I. Number pf lipids (N_{lipids}), with RSMF smaller than 3.0 Å, attached to the protein for the whole production run in the RX450 and RY200 replicas for models A, B and C.

Model	Lipid Species	N_{lipids} (RX450)	N_{lipids} (RY200)
A	POPC	5	8
	POPE	0	0
	CHL	0	0
	ALL	5	8
B	POPC	2	3
	POPE	1	2
	CHL	2	2
	ALL	5	7
C	POPC	3	6
	POPE	2	4
	CHL	4	6
	ALL	9	16

Binding events are specific of the sampling of the isothermal-isobaric ensemble due to the stochastic nature of lipid diffusion with Langevin thermostat and barostat of each simulation. Their number is larger in the replica RY200 with respect to RX450, as expected due to the shorter time scale of the former. Interestingly, this number significantly increases, almost doubling, for model C which contains all three lipid species, in both RX200 and RY450, independently on the time scale. This is also reflected by the fact that the highest rightmost histograms in Fig. 3 are for model C in both RX450 and RY200, and fits well with the increased viscosity due to cholesterol content. Thus, the content of cholesterol is an important bulk property of the membrane that in turn promotes the persistence of lipid-protein binding events, for any lipid species.

The binding sites of each lipid with persistent binding to the receptor involved one or more protein sections (the helices M1, M2, M3, M4, the M2-M3 loop or the Cys-loop) of one or two adjacent subunits, and are reported in Tables II and III.

While being persistently bound to one or more specific helices/loops, the lipid molecules involved in these binding events can sporadically reach out for adjacent sections of the protein as well. Both the outermost M4 helices of each subunit and the space in-between adjacent subunits (e.g. in-between M1 and M3 helices) give rise to convenient binding sites; moreover, M4 helices contain CRAC and CARC motifs which are suitable sites for binding cholesterol (as reported in Table 3 in the SI). Most lipid persistent binding is to a single helix; however lipids, especially the two-tailed POPC and POPE, can bind across helices, resulting in a variety of poses. Representative examples are shown in Fig. 4 and described below

TABLE II. Lipid binding sites to the receptor (replicas RX450), characterised by one or more helices/loops of one or two subunits (indicated as subscripts). The sites reported are only those whose corresponding lipid residue has a RMSF below 3.0 Å. Selected binding sites are represented in Fig. 4.

Lipid	Binding site	
Model A, RX450		
POPC	$M1_2$ $M3_2$	
	$M1_1$ $M3_1$ $M4_1$	
	$M1_5$ $M3_1$ $M4_5$	
	$M1_3$ $M3_4$	
	$M4_2$	
Model B, RX450		
POPC	$M1_1$	
	$M1_3$	
POPE	$M1_4$ $M4_4$	
CHL	$M1_5$ $M4_5$	Fig.4a)
	$M1_4$ $M3_5$	
Model C, RX450		
POPC	$M4_1$	
	$M1_5$ $M4_5$	
	$M3_4$	
POPE	$M1_1$ $M4_1$	Fig. 4b)
	$M1_1$	Fig. 4c)
CHL	$M1_3$ $M4_3$	
	$M3_5$ $M4_5$	Fig. 4d)
	$M1_4$ $M3_5$	
	$M3_2$	

TABLE III. Lipid binding sites to the receptor (replicas RY200), characterised by one or more helices/loops of one or two subunits (indicated as subscripts). The sites reported are only those whose corresponding lipid residue has a RMSF below 3.0 Å. Selected binding sites are represented in Fig. 4.

Lipid	Binding site	
Model A, RY200		
POPC	$M1_1$ M2-M3 $loop_2$	
	$M4_4$	
	$M4_5$	
	$M1_4$ $M3_4$ $M4_4$ Cys-$loop_4$	
	$M1_5$ $M4_5$	
	$M1_3$ $M3_4$	
	$M4_3$	
	$M4_5$	
Model B, RY200		
POPC	$M1_1$ $M4_1$	
	$M3_2$ $M4_2$	
	$M4_5$	
POPE	$M1_2$ $M2_3$ $M3_3$ M2-M3$loop_3$	Fig. 4e)
	$M1_3$ $M3_4$ $M4_3$	
CHL	$M4_5$	
	$M3_5$	
Model C, RY200		
POPC	$M1_5$ $M4_5$ Cys-$loop_5$	Fig. 4f)
	$M1_4$	
	$M3_4$	
	$M3_4$	
	$M4_2$	
	$M3_3$ $M4_3$	
POPE	$M1_1$ $M3_1$ $M4_1$	Fig. 4g)
	$M1_1$ $M3_2$	
	$M1_5$	
	$M3_5$ $M4_5$	
CHL	$M3_2$	
	$M1_3$	
	$M3_2$	
	$M3_2$	
	$M1_1$ $M3_2$	
	$M3_4$	

(subscripts 1 to 5 are used to label the subunits).

In model B, RX450, a cholesterol molecule is bound to $M1_5$ and to $M4_5$, and is, for a certain fraction of the simulation, also able to partially intercalate within them to reach out for $M3_5$ (Fig. 4 a). In model C, RX450, a POPE phospolipid is bound to $M1_1$ and to $M4_1$, and intercalates within them to reach out for $M3_5$ for a fraction of time with one of its tails (Fig. 4 b), while another POPE is bound to $M1_1$, and at times its head penetrates in the direction of the innermost $M2_1$ (Fig. 4 c), forming a hydrogen bond with Leu273 which belongs to the M2-M3 loop and is immediately next to Pro274 which is highly conserved through the Cys-loop superfamily, as previously mentioned;[54] a cholesterol molecule is at a bound position that may lead to intercalation within the M1, M3 and M4 of subunit 5 (Fig. 4 d). In model B, RY200, one tail of a POPE phospolipid is able to intercalate between $M1_2$ and $M3_3$ and to reach out for the M2 helices of both subunits 2 and 3 (Fig. 4 e). In model C, RY200, a POPC phospolipid intercalates between $M1_5$ and $M4_5$ with one of its tails, which is at times able to reach out for $M2_5$ (Fig. 4 f); a POPE phospolipid binds to M1 and M4 of subunit 3, and reaches out with one of its tails to M3 of the same subunit, thus intercalating in the TMD, although without reaching the M2 helix (Fig. 4 g). It is also worth mentioning that intercalation events within the TMD also briefly occur for other, more mobile, lipids.

Overall, POPC and POPE are the lipids which intercalate the most thanks to the length and flexibility of their tails.

It is also interesting to notice how the binding sites are similar among the three models, this is not surprising since such sites would be specific to the protein and to the three lipid species investigated. However, as previously stated, a binding event in any of these sites becomes more likely to be observed for the model membrane with higher cholesterol contents.

POPC has been previously found to intercalate within the TMD of membrane proteins, e.g. GLIC,[33] and cholesterol binding events were shown to occur in the adenosine receptor type 2A,[43] the G-protein coupled 5-HT_{1B} receptor,[44] the $GABA_A$ receptor,[27] and ELIC.[31] Cholesterol, together with POPC and SDPC, intercalation within the four helices in one subunit of the 5-HT_{3A} receptor was observed over many microsecond timescale. A lipid-M2 interaction was, instead, registered for the $GABA_A$ receptor, although the cholesterol binding was in this case achieved through docking rather than via diffusion.[27]

At the membrane-protein interface, a variety of interactions favour a closer proximity between lipids and receptor. Given

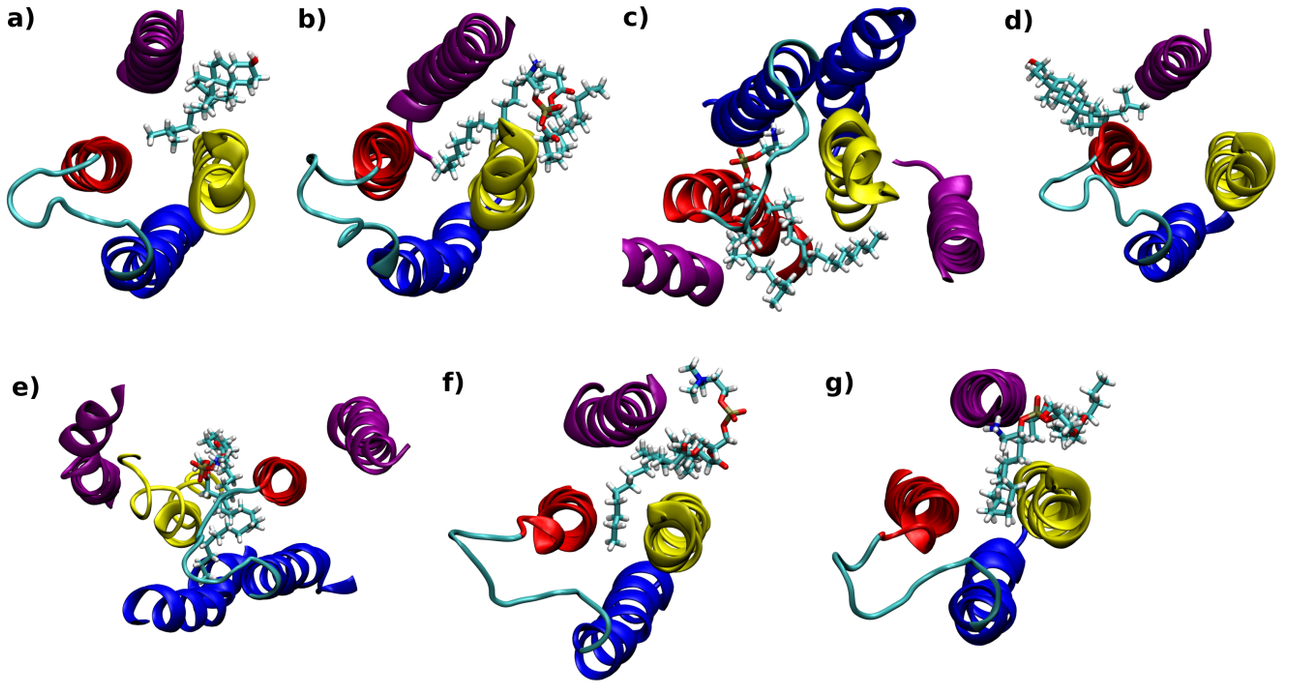

FIG. 4. Examples of persistent lipid binding to 5-HT_{3A}R: a) a CHL in model B; a POPE in model C; another POPE in model C; d) a CHL in model C in RX450 (Table II). e) a POPE in model B; f) a POPC in model C; and g) a POPE in model C in RY200 (Table III)The helices are coloured in yellow (M1), blue (M2), red (M3) and purple (M4) irrespective of the subunit they belong.

the statistical nature of how the lipid molecules diffuse, and their random distribution around the protein, a different local lipid environment is expected to surround each of the five receptor subunits, increasing the sampling. Lipids proximity to the helices of the TMD is affected by membrane viscosity and pressure, hydrogen bonds, hydrophobic effects, van der Waals and electrostatic interactions, etc. A generic contact between two given atoms (of two different residues) can be identified when their distance is shorter than a given cutoff; here we used a cut-off of 3.5 Å in agreement to previous studies.[76] The average number of contacts between a given helix/loop and a given lipid species (e.g. M1-POPC) were calculated for the five subunits, and for the three models. Their averages over the five subunits are shown in Fig. 5.

Fig. 6 shows the number of hydrogen bonds (averaged over time and subunits), grouped for every lipid species and protein section, including the four TMD helices M1, M2, M3 and M4, the M2-M3 loop and the Cys-loop.

The M1 helices are able to form contacts with lipids, very few of which are hydrogen bonds. Similarly, M2s form no hydrogen bonds, and only have sporadic contacts with the lipids, as expected due to their position deep within the protein. As for M3 and M4, both are able to form contacts and hydrogen bonds with the lipids, mostly with POPC. As for the M2-M3 loop and the Cys-loop, their location puts them in the position to interact with the upper leaflet's heads, thus via hydrogen bonds.

While no major differences are observed neither among the three models nor between the averaging methods, several interesting comments can be made regarding how hydrogen bonds are formed between POPC, POPE, cholesterol and the receptor. It is not surprising that most hydrogen bonds are formed with the outermost M4 helices, while their number is lower for the M3 and even less for the M1, both of which lie at the interface between adjacent subunits and so are less exposed to the membrane. The hydrogen bonds of M4 with POPC are more frequent in model A as expected due to its higher concentration, while the largest average number of hydrogen bonds with M4 is for model B, due to the increased hydrogen bonding ability of POPE. Notably, lipid molecules are able to reach out for the ECD, specifically interacting with the Cys-loop, and the M2-M3 loop connecting the M2 and M3 helices. Both these structures are thought to be critical for the receptor activation mechanism.[54,77,78] The average number of hydrogen bonds with the M2-M3 loop for any lipid species is larger for model C and the large error bars are indicative of the variability among subunits. As for the hydrogen bonds with the Cys-loop, both model B and model C dominate over model A when considering any lipid, while model A have obviously the largest number when considering POPC alone. POPC seems to be slightly more prone to engage in hydrogen bonds with the M2-M3 loop with respect to POPE, while the opposite appear to be true for the Cys-loop. A phospholipid in close proximity with the Cys-loop and the M2-M3 loop may engage in alternate, or even simultaneous hydrogen bonds with them, thus providing a bridge between these two key structures, as shown in the MD snapshot of Fig. 7. As for cholesterol, it appears to be less able to directly interact

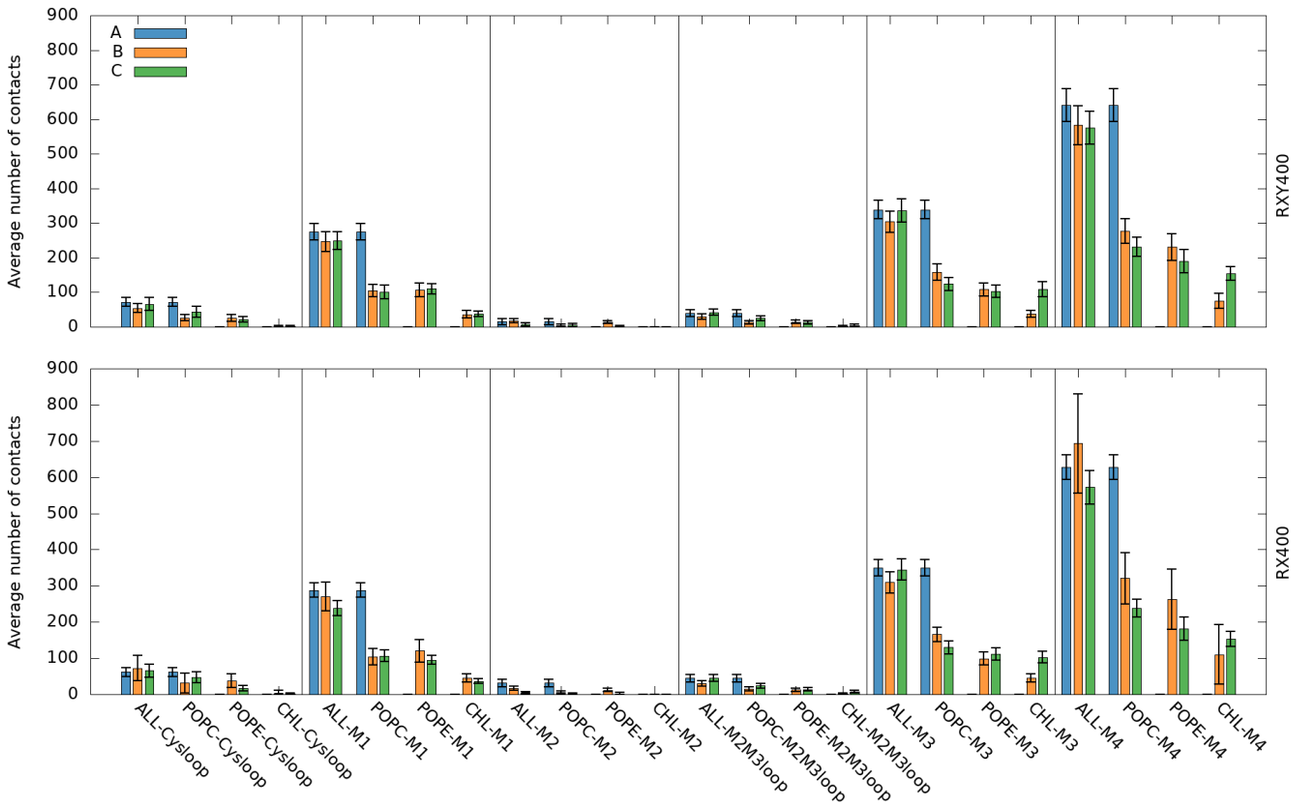

FIG. 5. Number of contacts, averaged over the five subunits, between helices/loops and lipids, for RXY400 (top) and for RX400 (bottom). Errors are calculated as standard deviations over the whole data sets at all time steps and then propagated for the five subunits.

with both the Cys-loop and the M2-M3 loop through hydrogen bonds than the phospolipids.

The average hydrogen bonds between the residues of these two loops and lipids are shown in Tables 1 and 2 in the SI. Two residues in the M2-M3 loop are particularly interesting: Thr280, which lies next to Pro281, whose *trans-cis* isomerisation may be linked to gating[54,77,78] and formed hydrogen bonds with lipids in each model, and Leu273, which is next to Pro274, a highly-conserved residue within the Cys-loop superfamily[9] which may also be important for gating because of its interaction with the $\beta 1$-$\beta 2$ loop.[7,9,79–81] In model C, sporadic hydrogen bonds are observed between Leu273 and POPE in subunit 2. However, Thr280 forms hydrogen bonds with lipids in all subunits, in particular with phospholipids, while only interacting with cholesterol in two subunits.

IV. DISCUSSION AND CONCLUSIONS

In this work, we performed molecular dynamics simulations to assess the effects of the model membrane composition at the interface with the 5-HT_{3A} receptor, a prototypical pLGIC for which anecdotal evidence suggests sensitivity to the lipid environment although the evidence insufficient to draw clear conclusions.[18] We compared a pure POPC model membrane and two different mixed ones, which also include POPE and cholesterol. These three models allowed us to distinguish the effects due to the mere presence of a lipid species in the membrane from those due to the specific lipid concentration, which spans the lower and upper limits of cholesterol concentration in synaptic membranes.

We tested two different ways to calculate statistical averages, one with two shorter replicas, and one with a single longer (i.e. double time) replica. Both methods gave similar results with no significant qualitative difference. While, due to the stochastic nature of lipid diffusion, the lipid environment around the receptor subunits depends on the specific replica and simulation time scale, qualitative trend can be inferred, further enhanced by the pentameric nature of the homomeric receptor, with five homomeric subunits in representative local environments at any given time.

The time scales simulated here are representative of the process of lipid diffusion and rearrangements within the membrane and around this complex protein, which occur on tens to hundreds of nanoseconds,[61,62] and thus provide a meaningful statistics of the lipid-protein interactions and contacts.

A variety of binding events between the protein and both phospholipids and cholesterol were observed in the simulations. The model with highest viscosity, i.e. the one with highest cholesterol content, also results to be the one with the highest number of binding events. The binding sites involved one or more of the helices/loops of one or two adjacent subunits,

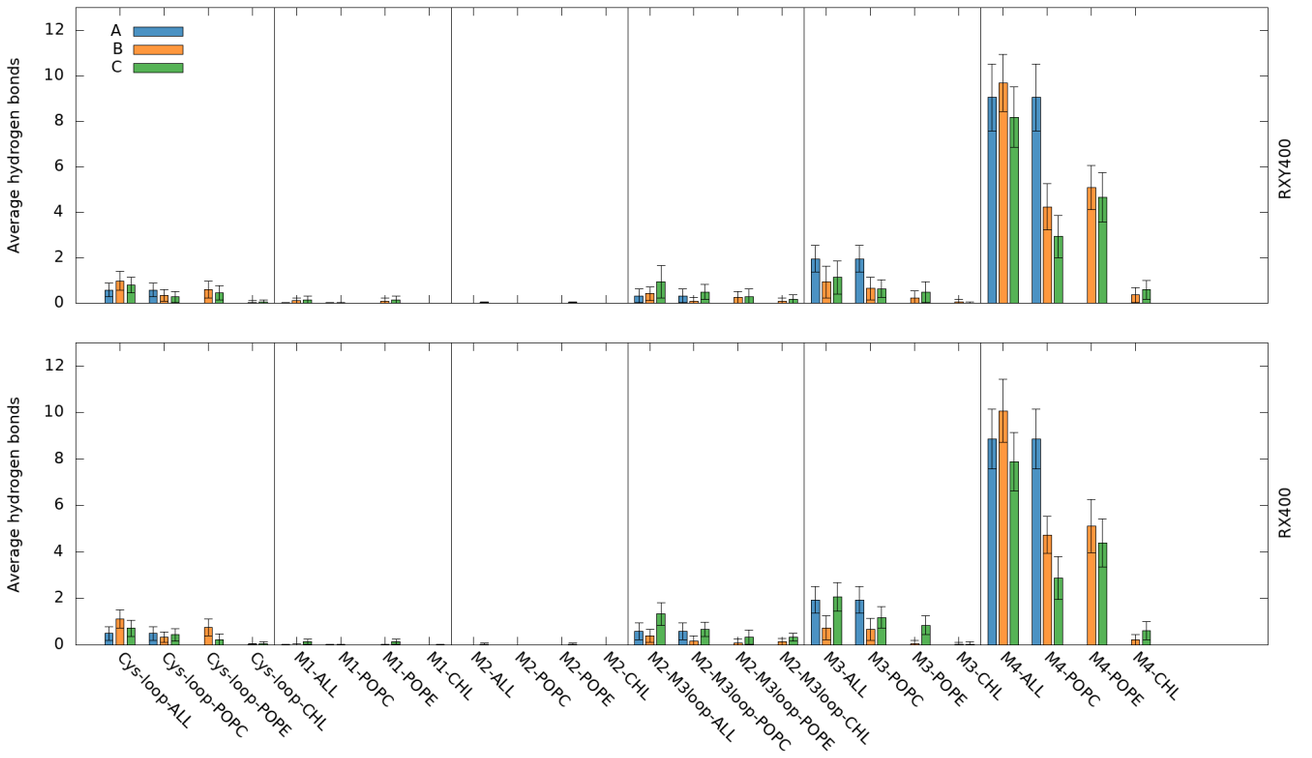

FIG. 6. Average number of hydrogen bonds between receptor and lipids for RXY400 (top) and for RX400 (bottom). Errors are calculated as standard deviations over the whole data sets at all time steps and then propagated for the five subunits.

and at times led to intercalation in the TMD, either within the helices of one subunit or within the grooves between two adjacent ones, potentially reaching for inner structures.

Our results highlight the relative importance of phospholipids with respect to cholesterol and vice-versa, with the different species competing for binding. Cholesterol abundance in the membrane affects its viscosity, while, thanks to their higher number of suitable moieties, phospholipids form the largest number of hydrogen bonds and are more able to intercalate within the protein, due to the length and/or flexibility of their tails, more likely to reach out for out-of-hand structures such as the Cys-loop in the ECD and the M2-M3 loop in the TMD, possibly acting as a bridge between these structures. The M2-M3 loop and the Cys-loop are thought to be involved in the signalling transmission chain of events between ligand binding and channel gating,[54,77] thus are important sections of the protein. Cholesterol is crucial: experimentally its depletion affects the distribution on the cell surfaces of 5-HT_{3A}R, as well as of other pLGICs; it also reduces serotonin-induced current response and desensitisation rates.[18]

Our study focussed on a non-conductive apo-state state and, within the simulated time (as well as much longer time scales[26]) the receptor structure was stable and did not changed significantly.

In conclusion, we have highlighted the role of cholesterol in tuning the properties of the membrane and therefore indirectly promoting lipid contacts and binding events to the receptor and giving the opportunity to phospholipids to mediate the connection between ECD and TMD, e.g. through the Cys-loop and the M2-M3 loop.

Although the available data are still limited to build a definitive picture of the role played by the lipid-5-HT_{3A}R interactions,[18] our results contribute to the understanding of this phenomena, shedding light on the behaviour of lipids in close proximity to the receptor at the atomistic level. A range of other simulations can be envisaged, e.g. spanning longer time scales, more accurate force-fields,[82], different functional states,[28] a larger variety of membrane compositions or many additional replicas starting from random initial lipid arrangements. Moreover, enhanced sampling methods may be used to induce/accelerate lipid intercalation or binding.[83]

V. CONFLICTS OF INTEREST

There are no conflicts to declare.

VI. ACKNOWLEDGEMENTS

We are grateful for computational support from the UK high performance computing service ARCHER, for which access was obtained via the UKCP consortium and funded by EPSRC grant EP/P022472/1. We also acknowledge the UK

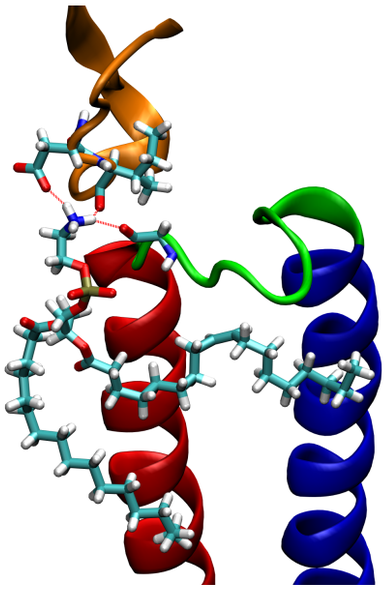

FIG. 7. A POPE lipid forms hydrogen bonds with residues of the M2-M3 loop (in green; Gly279) and of the Cys-loop (in orange; Asp138 and Ile139) simultaneously in model B, replica RY200.

Materials and Molecular Modelling Hub for computational resources, which is partially funded by EPSRC (EP/P020194/1). We thank Susanne Mesoy (University of Cambridge), Jemma Trick and Chris Lorenz (King's College London) for useful discussions.

The data supporting this research will be openly available from the King's College London research data archive.

[1] D. Lemoine, R. Jiang, A. Taly, T. Chataigneau, A. Specht and T. Grutter, *Chemical Reviews*, 2012, **112**, 6285–318.
[2] Á. Nemecz, M. S. Prevost, A. Menny and P.-J. Corringer, *Neuron*, 2016, **90**, 452–70.
[3] R. J. C. Hilf and R. Dutzler, *Nature*, 2009, **457**, 115–118.
[4] N. Bocquet, H. Nury, M. Baaden, C. Le Poupon, J.-P. Changeux, M. Delarue and P.-J. Corringer, *Nature*, 2009, **457**, 111–114.
[5] L. Sauguet, A. Shahsavar, F. Poitevin, C. Huon, A. Menny, À. Nemecz, A. Haouz, J.-P. Changeux, P.-J. Corringer and M. Delarue, *Proceedings of the National Academy of Sciences of the United States of America*, 2014, **111**, 966–971.
[6] P. S. Miller and A. R. Aricescu, *Nature*, 2014, **512**, 270–275.
[7] T. Althoff, R. E. Hibbs, S. Banerjee and E. Gouaux, *Nature*, 2014, **512**, 333–337.
[8] G. Hassaine, C. Deluz, L. Grasso, R. Wyss, M. B. Tol, R. Hovius, A. Graff, H. Stahlberg, T. Tomizaki, A. Desmyter, C. Moreau, X.-D. Li, F. Poitevin, H. Vogel and H. Nury, *Nature*, 2014, **512**, 276–281.
[9] X. Huang, H. Chen, K. Michelsen, S. Schneider and P. L. Shaffer, *Nature*, 2015, **526**, 277–280.
[10] J. Du, W. Lü, S. Wu, Y. Cheng and E. Gouaux, *Nature*, 2015, **526**, 224–229.
[11] M. Kudryashev, D. Castaño-Díez, C. Deluz, G. Hassaine, L. Grasso, A. Graf-Meyer, H. Vogel and H. Stahlberg, *Structure*, 2016, **24**, 165–170.
[12] M. Nys, E. Wijckmans, A. Farinha, Ö. Yoluk, M. Andersson, M. Brams, R. Spurny, S. Peigneur, J. Tytgat, E. Lindahl and C. Ulens, *Proceedings of the National Academy of Sciences of the United States of America*, 2016, **113**, E6696–E6703.
[13] S. Zhu, C. M. Noviello, J. Teng, R. M. Walsh, J. J. Kim and R. E. Hibbs, *Nature*, 2018, **559**, 67–72.
[14] S. Basak, Y. Gicheru, A. Samanta, S. K. Molugu, W. Huang, M. l. d. Fuente, T. Hughes, D. J. Taylor, M. T. Nieman, V. Moiseenkova-Bell and S. Chakrapani, *Nature Communications*, 2018, **9**, 514.
[15] S. Basak, Y. Gicheru, S. Rao, M. S. P. Sansom and S. Chakrapani, *Nature*, 2018, **563**, 270–274.
[16] L. Polovinkin, G. Hassaine, J. Perot, E. Neumann, A. A. Jensen, S. N. Lefebvre, P.-J. Corringer, J. Neyton, C. Chipot, F. Dehez, G. Schoehn and H. Nury, *Nature*, 2018, **563**, 275–279.
[17] V. Corradi, B. I. Sejdiu, H. Mesa-Galloso, H. Abdizadeh, S. Y. Noskov, S. J. Marrink and D. P. Tieleman, *Chemical Reviews*, 2019, **119**, 5775–5848.
[18] M. J. Thompson and J. E. Baenziger, *Biochimica et Biophysica Acta (BBA) - Biomembranes*, 2020, 183304.
[19] C. J. Baier, J. Fantini and F. J. Barrantes, *Scientific Reports*, 2011, **1**, 69.
[20] F. Barrantes, *Brain Research Reviews*, 2004, **47**, 71 – 95.
[21] G. Brannigan, J. Hénin, R. Law, R. Eckenhoff and M. L. Klein, *Proceedings of the National Academy of Sciences of the United States of America*, 2008, **105**, 14418–14423.
[22] J. E. Baenziger, J. A. Domville and J. D. Therien, in *Sterol Regulation of Ion Channels*, ed. I. Levitan, Academic Press, 2017, vol. 80 of Current Topics in Membranes, pp. 95 – 137.
[23] F. J. Barrantes, *Journal of Neurochemistry*, 2007, **103**, 72–80.
[24] C. J. B. daCosta and J. E. Baenziger, *The Journal of Biological Chemistry*, 2009, **284**, 17819–17825.
[25] C. J. B. daCosta, L. Dey, J. P. D. Therien and J. E. Baenziger, *Nature Chemical Biology*, 2013, **9**, 701–707.
[26] N. B. Guros, A. Balijepalli and J. B. Klauda, *Proceedings of the National Academy of Sciences of the United States of America*, 2020, **117**, 405–414.
[27] J. Hénin, R. Salari, S. Murlidaran and G. Brannigan, *Biophysical Journal*, 2014, **106**, 1938 – 1949.
[28] M. A. Dämgen and P. C. Biggin, *bioRxiv*, 2020.
[29] P. Kumar, Y. Wang, Z. Zhang, Z. Zhao, G. D. Cymes, E. Tajkhorshid and C. Grosman, *Proceedings of the National Academy of Sciences of the United States of America*, 2020, **117**, 1788–1798.
[30] A. Tong, J. T. n. Petroff, F.-F. Hsu, P. A. Schmidpeter, C. M. Nimigean, L. Sharp, G. Brannigan and W. W. Cheng, *eLife*, 2019, **8**, e50766.
[31] C. M. Hénault, C. Govaerts, R. Spurny, M. Brams, A. Estrada-Mondragon, J. Lynch, D. Bertrand, E. Pardon, G. L. Evans, K. Woods, B. W. Elberson, L. G. Cuello, G. Brannigan, H. Nury, J. Steyaert, J. E. Baenziger and C. Ulens, *Nature Chemical Biology*, 2019, **15**, 1156–1164.
[32] S. Basak, N. Schmandt, Y. Gicheru and S. Chakrapani, *eLife*, 2017, **6**, e23886.
[33] S. A. Heusser, M. Lycksell, X. Wang, S. E. McComas, R. J. Howard and E. Lindahl, *Proceedings of the National Academy of Sciences of the United States of America*, 2018, **115**, 10672–10677.
[34] S. M. Patra, S. Chakraborty, G. Shahane, X. Prasanna, D. Sengupta, P. K. Maiti and A. Chattopadhyay, *Molecular Membrane Biology*, 2015, **32**, 127–137.
[35] M. I. Mahmood, X. Liu, S. Neya and T. Hoshino, *Chemical and Pharmaceutical Bulletin*, 2013, **61**, 426–437.
[36] M. Jafurulla, B. D. Rao, S. Sreedevi, J.-M. Ruysschaert, D. F. Covey and A. Chattopadhyay, *Biochimica et biophysica acta*, 2014, **1838**, 158–163.
[37] R. Dawaliby, C. Trubbia, C. Delporte, M. Masureel, P. Van Antwerpen, B. K. Kobilka and C. Govaerts, *Nature chemical biology*, 2016, **12**, 35–39.
[38] D. E. Elmore and D. A. Dougherty, *Biophysical journal*, 2003, **85**, 1512–1524.
[39] L. Dominguez, L. Foster, J. E. Straub and D. Thirumalai, *Proceedings of the National Academy of Sciences of the United States of America*, 2016, **113**, E5281–E5287.
[40] P. V. Escribá, A. Ozaita, C. Ribas, A. Miralles, E. Fodor, T. Farkas and J. A. García-Sevilla, *Proceedings of the National Academy of Sciences of the United States of America*, 1997, **94**, 11375–11380.
[41] H. I. Ingólfsson, M. N. Melo, F. J. van Eerden, C. Arnarez, C. A. Lopez, T. A. Wassenaar, X. Periole, A. H. de Vries, D. P. Tieleman and S. J. Marrink, *Journal of the American Chemical Society*, 2014, **136**, 14554–14559.
[42] S. J. Marrink, V. Corradi, P. C. Souza, H. I. Ingólfsson, D. P. Tieleman and M. S. Sansom, *Chemical Reviews*, 2019, **119**, 6184–6226.
[43] R. Cao, G. Rossetti, A. Bauer and P. CarIoni, *PLOS ONE*, 2015, **10**, 1–13.
[44] V. Oakes and C. Domene, *Journal of Molecular Biology*, 2019, **431**, 1633 – 1649.
[45] R. B. Chan, T. G. Oliveira, E. P. Cortes, L. S. Honig, K. E. Duff, S. A. Small, M. R. Wenk, G. Shui and G. Di Paolo, *The Journal of biological chemistry*, 2012, **287**, 2678–2688.
[46] F. W. Pfrieger, *Biochimica et Biophysica Acta (BBA) - Biomembranes*,

2003, **1610**, 271 – 280.
[47]A. Filippov, G. Orädd and G. Lindblom, *Biophysical journal*, 2003, **84**, 3079–3086.
[48]H. Li and V. Papadopoulos, *Endocrinology*, 1998, **139**, 4991–4997.
[49]J. Fantini and F. J. Barrantes, *Frontiers in physiology*, 2013, **4**, 31–31.
[50]J. Fantini, C. Di Scala, L. S. Evans, P. T. F. Williamson and F. J. Barrantes, *Scientific reports*, 2016, **6**, 21907–21907.
[51]D. Di Maio, B. Chandramouli and G. Brancato, *PLOS ONE*, 2015, **10**, 1–23.
[52]S. Yuan, S. Filipek and H. Vogel, *Structure*, 2016, **24**, 816–825.
[53]M. Y. Antonov, A. V. Popinako and G. A. Prokopiev, *AIP Conference Proceedings*, 2016, **1773**, 060001.
[54]A. Crnjar, F. Comitani, W. Hester and C. Molteni, *The Journal of Physical Chemistry Letters*, 2019, **10**, 694–700.
[55]C. X. Weichenberger and M. J. Sippl, *Nucleic acids research*, 2007, **35**, W403–W406.
[56]S. Jo, T. Kim, V. G. Iyer and W. Im, *Journal of Computational Chemistry*, 2008, **29**, 1859–1865.
[57]J. Shan, G. Khelashvili, S. Mondal, E. L. Mehler and H. Weinstein, *PLoS computational biology*, 2012, **8**, e1002473–e1002473.
[58]J. C. Phillips, R. Braun, W. Wang, J. Gumbart, E. Tajkhorshid, E. Villa, C. Chipot, R. D. Skeel, L. Kalé and K. Schulten, *Journal of Computational Chemistry*, 2005, **26**, 1781–1802.
[59]J. A. Maier, C. Martinez, K. Kasavajhala, L. Wickstrom, K. E. Hauser and C. Simmerling, *Journal of Chemical Theory and Computation*, 2015, **11**, 3696–3713.
[60]C. J. Dickson, B. D. Madej, Å. A. Skjevik, R. M. Betz, K. Teigen, I. R. Gould and R. C. Walker, *Journal of Chemical Theory and Computation*, 2014, **10**, 865–879.
[61]D. J. Smith, J. B. Klauda and A. J. Sodt, *Living Journal of Computational Molecular Science*, 2018, **1**, 5966.
[62]C. Kandt, W. L. Ash and D. P. Tieleman, *Methods*, 2007, **41**, 475 – 488.
[63]W. V. Kraske and D. B. Mountcastle, *Biochimica et Biophysica Acta (BBA) - Biomembranes*, 2001, **1514**, 159 – 164.
[64]J. Silvius, *In: Jost PC, Griffith OH, editors. Lipid-Protein Interactions, John Wiley & Sons, Inc., NewYork*, 1982, 239–281.
[65]D. R. Roe and T. E. Cheatham, *Journal of Chemical Theory and Computation*, 2013, **9**, 3084–3095.
[66]N. Michaud-Agrawal, E. J. Denning, T. B. Woolf and O. Beckstein, *Journal of Computational Chemistry*, 2011, **32**, 2319–2327.
[67]R. J. Gowers, M. Linke, J. Barnoud, T. J. E. Reddy, M. N. Melo, S. L. Seyler, D. L. Dotson, J. Domanski, S. Buchoux, I. M. Kenney, and O. Beckstein, *Proceedings of the 15th Python in Science Conference*, 2016, 98–105.
[68]A. Crnjar, F. Comitani, C. Melis and C. Molteni, *Interface Focus*, 2019, **9**, 20180067.
[69]F. Comitani, N. Cohen, J. Ashby, D. Botten, S. C. R. Lummis and C. Molteni, *Journal of computer-aided molecular design*, 2014, **28**, 35–48.
[70]F. Comitani, C. Melis and C. Molteni, *Biochemical Society Transactions*, 2015, **43**, 151–6.
[71]F. Comitani, V. Limongelli and C. Molteni, *Journal of Chemical Theory and Computation*, 2016, **12**, 3398–3406.
[72]C. Melis, S. C. R. Lummis and C. Molteni, *Biophysical Journal*, 2008, **95**, 4115–4123.
[73]T. J. McCormack, C. Melis, J. Colon, E. A. Gay, A. Mike, R. Karoly, P. W. Lamb, C. Molteni and J. L. Yakel, *The Journal of Physiology*, 2010, **588**, 4415–4429.
[74]S. Moradi, A. Nowroozi and M. Shahlaei, *RSC Advances*, 2019, **9**, 4644–4658.
[75]S. Ramadurai, R. Duurkens, V. V. Krasnikov and B. Poolman, *Biophysical journal*, 2010, **99**, 1482–1489.
[76]S. S. Deol, P. J. Bond, C. Domene and M. S. Sansom, *Biophysical Journal*, 2004, **87**, 3737 – 3749.
[77]S. C. R. Lummis, D. L. Beene, L. W. Lee, H. A. Lester, R. W. Broadhurst and D. A. Dougherty, *Nature*, 2005, **438**, 248–252.
[78]C. Melis, G. Bussi, S. C. R. Lummis and C. Molteni, *The Journal of Physical Chemistry B*, 2009, **113**, 12148–53.
[79]N. Calimet, M. Simoes, J.-P. Changeux, M. Karplus, A. Taly and M. Cecchini, *Proceedings of the National Academy of Sciences of the United States of America*, 2013, **110**, E3987–E3996.
[80]Z.-S. Wu, H. Cheng, Y. Jiang, K. Melcher and H. E. Xu, *Acta Pharmacologica Sinica*, 2015, **36**, 895–907.
[81]I.-S. Chen and Y. Kubo, *The Journal of Physiology*, 2018, **596**, 1833–1845.
[82]G. Klesse, S. Rao, S. J. Tucker and M. S. Sansom, *Journal of the American Chemical Society*, 2020, **142**, 9415–9427.
[83]R. A. Corey, P. J. Stansfeld and M. S. Sansom, *Biochemical Society Transactions*, 2019, **48**, 25–37.

Biointerphases

PLEASE CITE THIS ARTICLE AS DOI: 10.1116/6.0000561

POPC

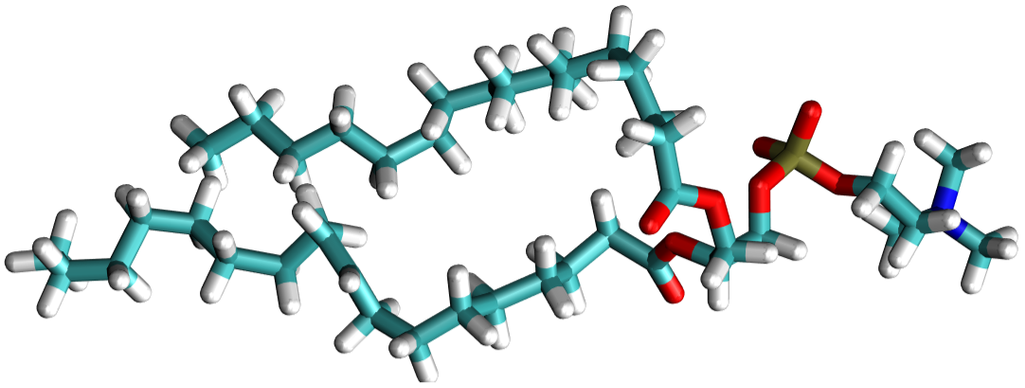

POPE

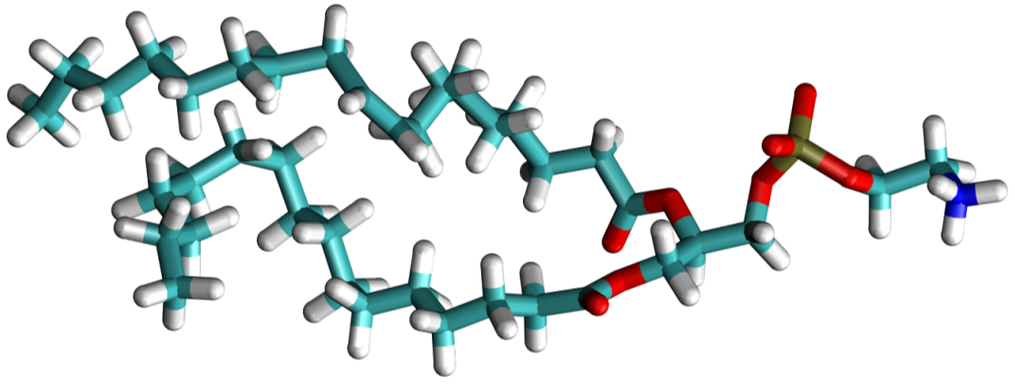

CHL

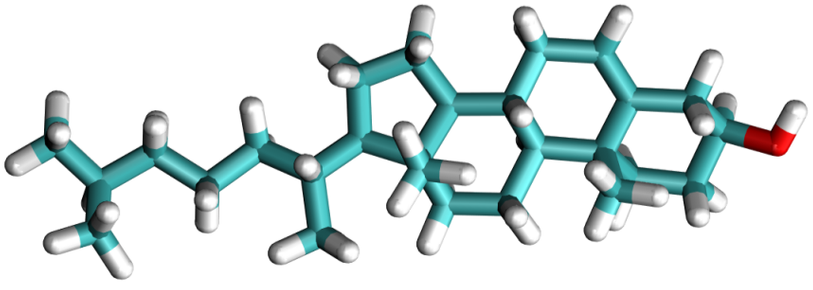

Biointerphases

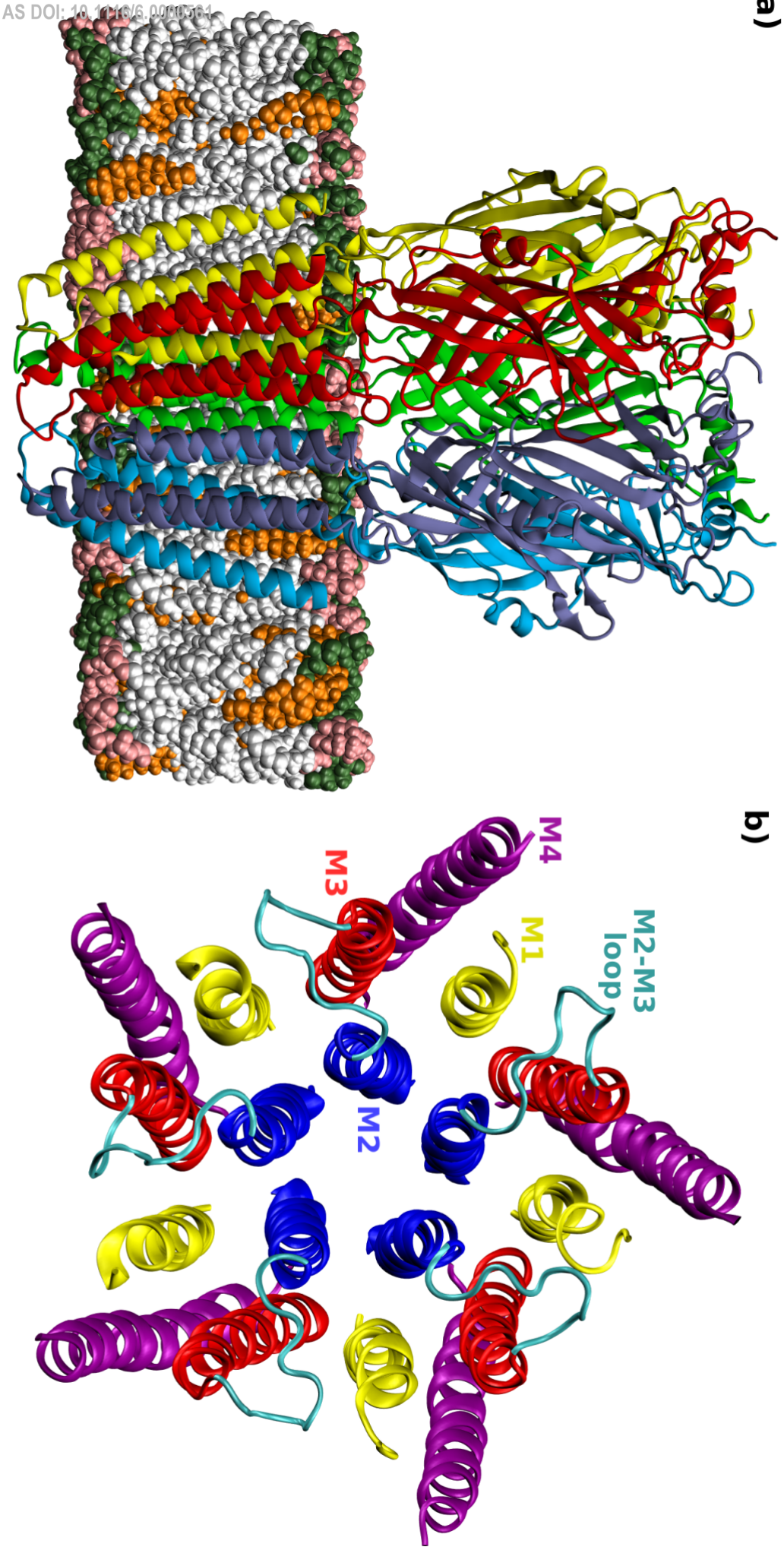

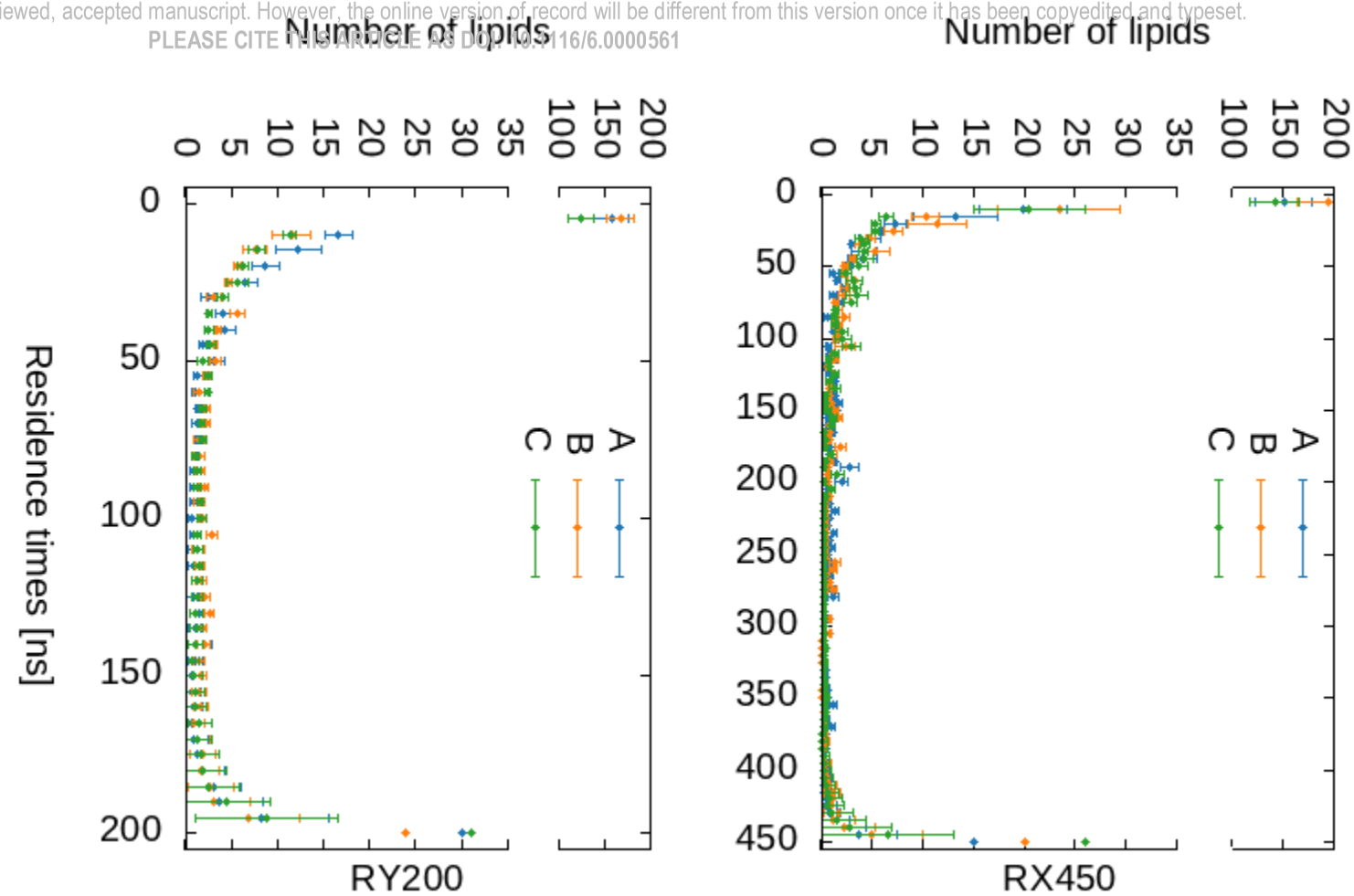

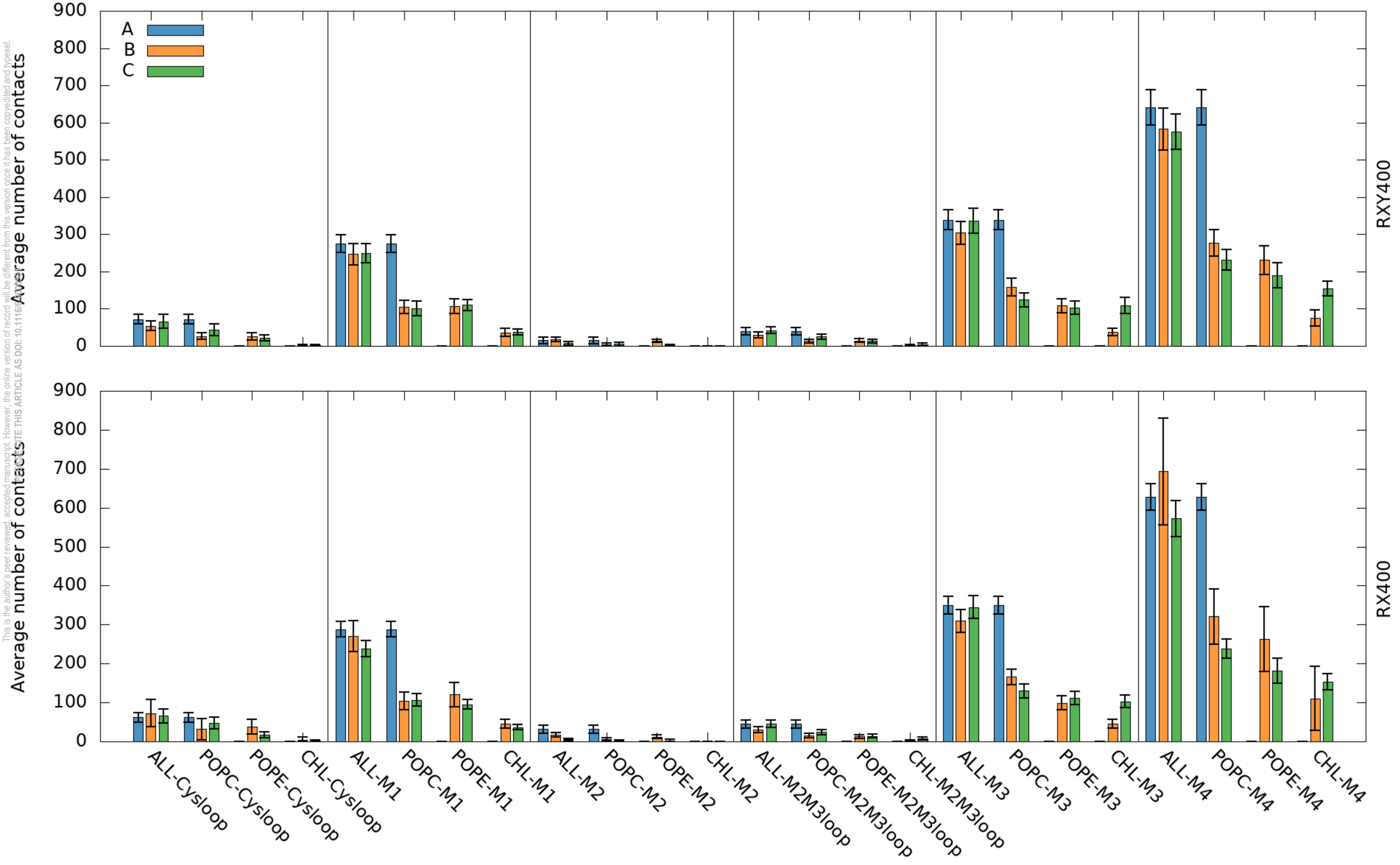

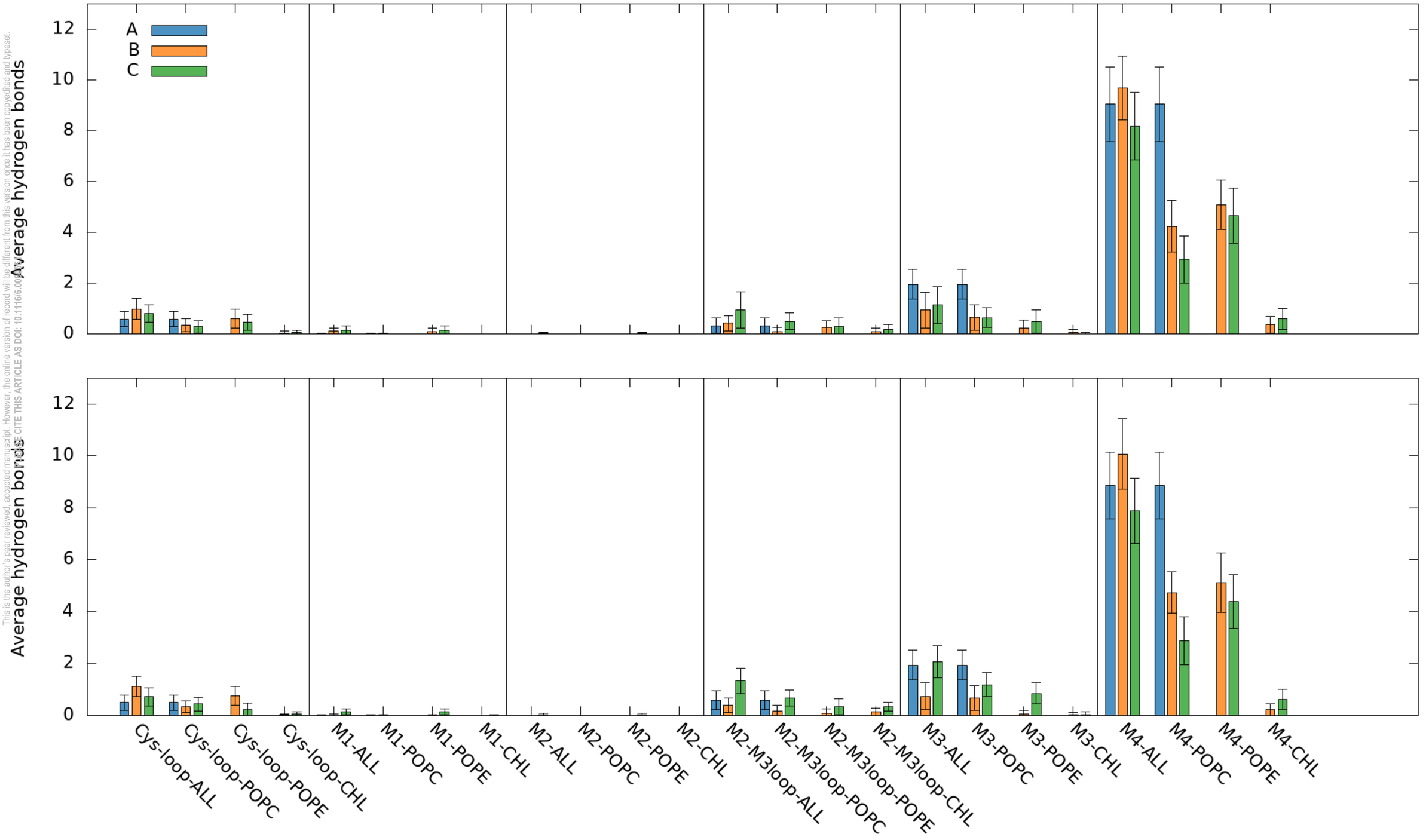

Biointerphases